Monthly Notices of the ROYAL ASTRONOMICAL SOCIETY

MNRAS **448,** 1704–1714 (2015) doi:10.1093/mnras/stv091

ExoMol line lists – VIII. A variationally computed line list for hot formaldehyde

Ahmed F. Al-Refaie,* Andrey Yachmenev, Jonathan Tennyson and Sergei N. Yurchenko

Department of Physics and Astronomy, University College London, Gower Street, WC1E 6BT London, UK

Accepted 2014 December 23. Received 2014 December 20; in original form 2014 December 3

ABSTRACT

A computed line list for formaldehyde, $H_2{}^{12}C^{16}O$, applicable to temperatures up to $T = 1500$ K is presented. An empirical potential energy and ab initio dipole moment surfaces are used as the input to the nuclear motion program TROVE. The resulting line list, referred to as *AYTY*, contains 10.3 million rotational-vibrational states and around 10 billion transition frequencies. Each transition includes associated Einstein-*A* coefficients and absolute transition intensities, for wavenumbers below 10 000 cm^{-1} and rotational excitations up to $J = 70$. Room-temperature spectra are compared with laboratory measurements and data currently available in the HITRAN data base. These spectra show excellent agreement with experimental spectra and highlight the gaps and limitations of the HITRAN data. The full line list is available from the CDS data base as well as at www.exomol.com.

Key words: molecular data – opacity – planets and satellites: atmospheres – stars: atmospheres – ISM: molecules.

1 INTRODUCTION

Formaldehyde, H_2CO, is a poisonous molecule in the aldehyde group. On Earth it plays a part in troposphere chemistry dynamics as the main source of OH via photodissociation and is formed from photo-oxidation in the atmosphere or through the incomplete burning of biomass (Wayne 2000). Traces of formaldehyde have tentatively been detected in the Martian atmosphere (Korablev et al. 1993) where it is believed to be derived from the oxidation of methane (CH_4; Villanueva et al. 2013).

Formaldehyde was the first polyatomic molecule to be detected in the interstellar medium (ISM; Zuckerman et al. 1970) and is extremely abundant (Langer 1976). This has made it useful in investigating the isotope composition of carbon in the galaxy (Zuckerman et al. 1974). The proposed mechanism of production is via the successive hydrogenation of CO (Woon 2002) on icy grain mantles:

$$\begin{aligned} \mathrm{H} + \mathrm{CO} &\rightarrow \mathrm{HCO} \\ \mathrm{H} + \mathrm{HCO} &\rightarrow \mathrm{H_2CO}. \end{aligned} \quad (1)$$

Further hydrogenation produces methanol through an intermediate methyl radical $H+H_2CO \rightarrow CH_3O \rightarrow H+CH_3O \rightarrow CH_3OH$. Common reactions include that with ammonia which produces amines (Schutte 2002) and polymerization with other H_2CO molecules. As a result, formaldehyde is believed to be the major precursor for the formation of complex organic molecules in the ISM that include interstellar glycolaldehyde (Hollis, Lovas & Jewell 2000) and amino acids (Schutte 2002).

Formaldehyde's astrophysical relevance does not end in the ISM. Recently, it has been detected in comets (Bockelee-Morvan & Crovisier 1992), such as 103P/Hartley 2 (Dello Russo et al. 2011), C/2007 N3 (Villanueva et al. 2011) and Hale-Bopp (Milam et al. 2006), where it is thought to originate from the degradation of polyoxymethylene (Cottin et al. 2001). It is also present in protoplanetary discs around low-mass young stars (Taurus-Auriga Class I/II; Zasowski et al. 2009; Öberg et al. 2010; Sargent et al. 2014) as circumstellar ice with an abundance ratio of ≈2 per cent compared to the more ubiquitous water ice.

Because of H_2CO's role as a precursor to complex organic molecules, it is considered a possible biomarker. The RNA world hypothesis suggests an early Earth with a CO_2-, H_2O- and N_2-rich atmosphere (Neveu, Kim & Benner 2013). Illuminating this mix with ultraviolet (UV) radiation should lead to a large amount of formaldehyde being fixed in the atmosphere before being deposited into the prebiotic oceans (Neveu et al. 2013). Alternatively, the source of prebiotic chemical compounds may be derived without need of illuminating UV radiation via glancing icy body impacts (Goldman & Tamblyn 2013). Such impacts would produce shock-compression conditions that lead to the formation of HCN molecules. These HCN molecules can be hydrolyzed to form formaldehyde and from there produce amino acids. Thus, a planet rich in formaldehyde may indicate one undergoing the stages of pre-life.

Finally, formaldehyde masers (Forster et al. 1980; Pratap, Snyder & Batrla 1992) are a reliable and proven tracer for high-density environments such as star-forming regions in galaxies due to its

* E-mail: ahmed.al-refaie.12@ucl.ac.uk

ubiquity and large number of long-wavelength transitions (Mangum et al. 2008). Currently, there are 19 extragalactic sources (Mangum et al. 2008), of these masers including IRAS 18566+0408, which is notable for detection of the first H_2CO maser flare (Araya et al. 2007). Formaldehyde masers (and maser flares) have mostly been observed via the $1_{10} \rightarrow 1_{11}$ and $2_{11} - 2_{12}$ *K*-doublet transitions at 6.1 and 2.2 cm, respectively.

The wide range of interactions in atmospheric, terrestrial, astrophysical and astrobiological phenomena make formaldehyde a relevant molecule in the chemistry of exoplanets and their atmospheres. Therefore, a complete, high-resolution, line list for H_2CO should provide an important aid for characterization and modelling of formaldehyde. These considerations led us to study formaldehyde as part of the ExoMol project (Tennyson & Yurchenko 2012), which aims to produce comprehensive molecular line lists for studies of the atmospheres of exoplanets and cool stars.

High-resolution, room-temperature formaldehyde spectra have been well studied in the laboratory (Johns & McKellar 1975; Brown, Hunt & Pine 1979; Nakanaga, Kondo & Saeki 1982; Nadler, Daunt & Reuter 1987; Cline & Varghese 1988; Reuter et al. 1989; Poulin et al. 1996; Theulé et al. 2003); the early work was reviewed by Clouthier & Ramsay (1983). Currently, the major source of publicly available spectroscopic data on H_2CO is the HITRAN data base (Rothman et al. 2013) which has recently been updated to include long-wavelength data from the CDMS data base (Müller et al. 2005). The spectral regions covered in the data bases are 0–100, 1600–1800 (Perrin et al. 2009) and 2500–3100 cm^{-1} (Perrin et al. 2009) at up to 10^{-29} cm per molecule sensitivity for $T = 296$ K. However, this accounts for only 40 000 transitions extending up to $J = 64$ and covers only four of the six fundamental vibrational bands as well as the ground-state rotational spectrum. This deficiency arises from an apparent lack of absolute intensities in the 100–1600 cm^{-1} range. Additional observed transitions are available (Perrin et al. 2009) and include line positions (Perrin, Keller & Flaud 2003; Tchana, Perrin & Lacome 2007; Zhao et al. 2007), and intensities (Perrin, Keller & Flaud 2003; Flaud et al. 2006; Perrin, Valentin & Daumont 2006) of some of the fundamental bands and hot bands (Ito, Nakanaga & Takeo 1994; Perez et al. 2006; Margules et al. 2009). The incompleteness and low rotational excitations available in HITRAN limit the applicability of these data for temperatures above 300 K. The theoretical spectra presented in this paper aim to provide a more complete and accurate picture of the spectra of formaldehyde up to 10 000 cm^{-1} and for temperatures up to 1500 K. Our line list should therefore be useful for modelling higher temperature environments as well as studies on non-local thermodynamic equilibrium transitions such as those observed in masers.

Theoretically, electric dipole transition intensities of H_2CO were studied by Luckhaus et al. (1996) and Carter et al. (2009); see also the review by Yurchenko (2014). Luckhaus et al. (1996) used an ab initio MP2/6-311G** dipole moment surface (DMS) to simulate the photoacoustic spectrum of high C-H stretching overtones of H_2CO. Carter et al. (2009) generated an ab initio couple-cluster CCSD(T)/aug-cc-pVTZ DMS for H_2CO; they used an effective representation of charges to compute (relative) ro-vibrational line intensities for H_2CO reproducing the HITRAN data (Rothman et al. 2009) with reasonable agreement. Poulin et al. (1996) computed an ab initio DMS using the QCISD/6-31111G(d,p) level of theory and presented it as an expansion.

Despite these works there is no comprehensive line list for formaldehyde available in the literature. The goal of this work is to bridge this gap. We use the variational program TROVE (Yurchenko, Thiel & Jensen 2007) in conjunction with an initial potential energy surface (PES) obtained 'spectroscopically' by Yachmenev et al. (2011) and a new ab initio DMS for formaldehyde and generate an extensive line list for $H_2{}^{12}C^{16}O$ applicable for the temperatures up to $T = 1500$ K. In the following, H_2CO and formaldehyde will refer to the main isotopologue $H_2{}^{12}C^{16}O$.

Table 1. Vibrational modes and observed band centres in cm^{-1} by Carter, Pinnavaia & Handy (1995).

Mode	Band centres	Symmetry	Description
ν_1	2782.46	A_1	Symmetric C-H stretching
ν_2	1746.01	A_1	C-O stretching
ν_3	1500.18	A_1	Symmetric O-C-H bending
ν_4	1167.26	B_1	Out-of-plane bending
ν_5	2843.33	B_2	Asymmetric C-H stretching
ν_6	1249.10	B_2	Asymmetric O-C-H bending

2 METHOD

2.1 Background

H_2CO is a prolate asymmetric top molecule that belongs to the C_{2v} molecular symmetry group (Bunker & Jensen 1998). The group has four irreducible representations A_1, A_2, B_1 and B_2. Once the H atom nuclear spin is taken into account, the 'para' *A* representations are singly degenerate and the 'ortho' *B* representations are triply degenerate. As H_2CO has four atoms, it has six vibrational modes; Table 1 shows the vibrational modes and their corresponding symmetries, band centres and descriptions. Coriolis interactions occur strongly between the ν_4 and ν_6 modes, and weakly between the ν_3 and ν_4 modes (Nakagawa & Morino 1971) which couples their energy levels and wavefunctions. This manifests itself in the ν_3, ν_4 and ν_6 mode interaction as overlapping bands which make these three bands difficult to distinguish from each other.

2.2 Potential energy surface

Full details of their PES calculation are given by Yachmenev et al. (2011), so only a brief summary is presented here. The initial PES was computed ab initio using the CCSD(T)/aug-cc-pVQZ theory. Variational calculations with this surface give a root-mean-square (rms) error of 5.1 cm^{-1} for the fundamental band centres. Yachmenev et al. (2011) refined the ab initio PES using a $V' = V + \Delta V$ formulation, where V, ΔV and V' are the original ab initio, correction and refined PES, respectively. The eigenfunctions of the original ab initio Hamiltonian, $H = T + V$, are used as the basis functions for the extended Hamiltonian $H' = H + \Delta V$, where ΔV is typically small and almost diagonal correction. ΔV is expanded in Taylor series and expansion coefficients are obtained in a variational least-squares fit to high-resolution spectroscopic data using TROVE. The rms error against experimental energy levels with $J \leq 5$ of this semi-empirical PES, called H2CO-2011, is 0.04 cm^{-1}.

It should be noted however that the excellent accuracy of the refined PES caused serious problems with the absolute intensities of some bands. The intensities based on the initial, less accurate ab initio PES, the intensities of the ν_3, ν_4 and ν_6 bands were observed to agree much better with the experiment. Fig. 1(a) highlights this effect, where an order-of-magnitude difference in absolute intensity and cross-section was observed. Initially blamed on the DMS, it

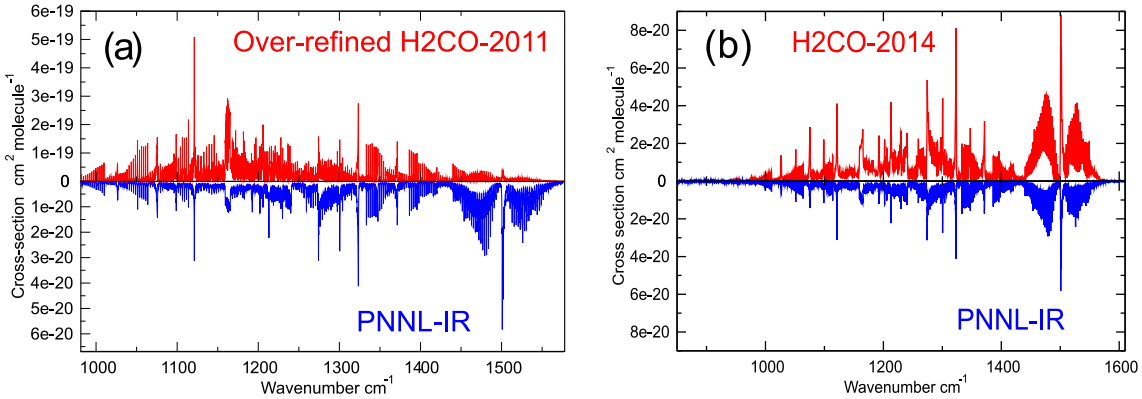

Figure 1. Overview of the ν_3, ν_4 and ν_6 region between different PES used in production and PNNL-IR (Sharpe et al. 2004) cross-sections: (a) represents the over-refined PES, (b) the 'better' refinement. Note the difference in y-axis scaling in (a) to highlight structural features.

was soon discovered that the original ab initio PES did not have this problem.

In order to address this issue, we have repeated the refinement process making it less aggressive with careful observation of the transition moments. In the present work, we have also increased the size of the basis set (see the discussion below). We used the same fitting set of experimental energies as well as the same functional form for PES. The rms deviation of the experimental term values used in the PES fit ($J \leq 5$) against the computed energies in AYTY is 0.18 cm^{-1} (0.006 cm^{-1} for pure rotational term values). The potential parameters as well as the associated FORTRAN 95 program are given as supplementary material. The resulting line intensities have returned to the quality of the ab initio levels as can be seen in Fig. 1(b).

2.3 Variational computation

The TROVE program suite (Yurchenko et al. 2007) is employed to compute our formaldehyde line list as well as to perform the least-squares fit of the ab initio PES discussed above. TROVE is designed to compute variational ro-vibrational energy levels, associated eigenfunctions and transition intensities for molecules of arbitrary structure. Variational methods are often limited in their efficiency due to the need to diagonalize increasingly large Hamiltonian matrices as the complexity of the molecule increases. However, with the improved computational power and parallelism of modern CPUs, it is now feasible to solve ro-vibrational Schrödinger equations for polyatomic molecules. TROVE has been successfully used to produce high-accuracy line lists and spectra for tetratomic molecules such as HSOH (Yachmenev et al. 2010), NH_3 (Yurchenko, Barber & Tennyson 2011), SO_3 (Underwood, Tennyson & Yurchenko 2013), PH_3 (Sousa-Silva, Yurchenko & Tennyson 2013; Sousa-Silva et al. 2015) and SbH_3 (Yurchenko et al. 2010), as well as recently the pentatomic molecule CH_4 (Yurchenko & Tennyson 2014).

TROVE approximates the kinetic energy operator (KEO) by a truncated Taylor series expansion in generalized coordinates. Previous calculations for H_2O_2 by Polyansky et al. (2013) show that computations using series representation of the KEO for non-linear molecules, such as H_2CO, converge as well as exact KEO-based programs such as WAVR4 (Kozin et al. 2004) and, particularly for excited rotational states, at the cost of significantly less computational time. In this work, we use a kinetic expansion order of 6 for optimal convergence while providing reasonable computation times and similarly, we use a potential energy expansion order of 8.

In TROVE, the primitive vibrational basis set is represented by a symmetrized product of six one-dimensional vibrational functions $\phi_{n_1}(r_1^\ell)$, $\phi_{n_2}(r_2^\ell)$, $\phi_{n_3}(r_3^\ell)$, $\phi_{n_4}(\theta_1^\ell)$, $\phi_{n_5}(\theta_2^\ell)$ and $\phi_{n_6}(\tau)$, where n_i denotes the associated local mode vibrational quanta, $\{r_1^\ell, r_2^\ell, r_3^\ell, \theta_1^\ell, \theta_2^\ell\}$ are linearized versions (Bunker & Jensen 1998; Yurchenko et al. 2007) of the coordinates $\{r_{\rm CO}, r_{\rm CH_1}, r_{\rm CH_2}, \theta_{\rm OCH_1}$ and $\theta_{\rm OCH_2}\}$, respectively, and τ is the dihedral angle between the OCH_1 and OCH_2 planes. The functions $\phi_{n_i}(q_i)$ are obtained by solving the corresponding 1D Schrödinger equation (Yurchenko et al. 2007) for the vibrational motion associated with the corresponding coordinate $q_i \in \{r_1^\ell, r_2^\ell, r_3^\ell, \theta_1^\ell, \theta_2^\ell, \tau\}$, with the other coordinates held fixed at their equilibrium values, where the Numerov–Cooley method (Noumerov 1924; Cooley 1961) is used. The direct product of the 1D basis functions is contracted using the polyad condition:

$$P = 2(n_2 + n_3) + n_1 + n_4 + n_5 + n_6 \leq P_{\rm max}, \quad (2)$$

which in terms of the normal mode quantum numbers v_i reads

$$P = 2(v_1 + v_5) + v_2 + v_3 + v_4 + v_6 \leq P_{\rm max}. \quad (3)$$

This polyad rule is based on the approximate relationship between the H_2CO fundamental frequencies (see Table 1):

$$\nu_1 \approx \nu_5 \approx 2\nu_2 \approx 2\nu_3 \approx 2\nu_4 \approx 2\nu_6. \quad (4)$$

The vibrational basis set is further optimized by solving four reduced eigenproblems variationally for $\{q_1\}$, $\{q_2, q_3\}$, $\{q_4, q_5\}$ and $\{q_6\}$ to produce four sets of wavefunctions $\Phi^{(1)}_{n_1}(q_1)$, $\Phi^{(2,3)}_{n_2,n_3}(q_2, q_3)$, $\Phi^{(4,5)}_{n_4,n_5}(q_4, q_5)$ and $\Phi^{(6)}_{n_6}(q_6)$, respectively. At step 2, the pure vibrational ($J = 0$) problem is solved variationally using the basis set constructed as a symmetrized direct product of $\Phi^{(i)}_{n_i}$ ($i = 1, 6$) and $\Phi^{(j,k)}_{n_j,n_k}$ ($j, k = 2, 3$ or 4, 5) contracted through the polyad number condition (2) and symmetrized according to the $C_{2v}(M)$ molecular symmetry group. In this work, the basis set is truncated at $P_{\rm max} = 16$ as the relative simplicity of the molecule means that this gives well-converged results. The maximum polyad number $P_{\rm max}$ restricts the number of combinations of $\phi^{(i)}_{n_i}$ and $\Phi^{(i,j)}_{n_i,n_j}$ for which $P \leq P_{\rm max}$. The resulting eigenfunctions $\Psi_i^{J=0,\Gamma}$ obtained for each $C_{2v}(M)$ symmetry $\Gamma = A_1, A_2, B_1$ and B_2 together with the symmetrized rigid rotor wavefunctions $|J, K, \tau_{\rm rot}\rangle$ form our $J = 0$ basis set representation (Yurchenko et al. 2009), where the ro-vibrational basis functions are given as a direct product of $\Psi_i^{J=0,\Gamma}$ and $|J, K, \tau_{\rm rot}\rangle$. Here $\tau_{\rm rot}$ is the rotational parity defined by Yurchenko et al. (2005b), and K is the projection of the angular momentum on the body-fixed axis z. The latter is defined according with the Eckart conditions (Eckart 1935) and is oriented approximately along the CO bond. In

$C_{2v}(M)$ symmetry, K and $\tau_{\rm rot}$ correlate with the customary K_a and K_c rotational quantum numbers as

$$K = K_a, \quad \tau_{\rm rot} = \mathrm{mod}(|K_a - K_c|, 2). \tag{5}$$

The vibrational part of the $J = 0$ basis set is truncated using the energy threshold of hc 18 000 cm^{-1} and thus consists of 2310, 1531, 1688 and 2112 functions for the A_1, A_2, B_1 and B_2 symmetries, respectively.

The resulting ro-vibrational Hamiltonian matrix in the $J = 0$ representation exhibits a block diagonal structure where each of four blocks represents an irreducible representation A_1, A_2, B_1 or B_2 and can be diagonalized independently. Each of these blocks displays a band-diagonal structure whose bandwidth and length are determined by the $J = 0$ basis set size and the level of rotational excitation, respectively.

In generating our line list, we employed an upper eigenvalue limit of 18 000 cm^{-1} as the intensity of transitions involving higher energy states is too weak to be important. The $J = 0$ matrix blocks produced by TROVE were on average of dimensions 1920 × 1920. The rule of thumb for the average size of a block for $J \geq 1$ is $1920(2J + 1)$. The largest J computed was $J = 70$ which required the diagonalization of matrices of the order of ≈300 000 for eigenvalues and eigenvectors. The linear algebra libraries LAPACK (Anderson et al. 1999) and SCALAPACK (Blackford et al. 1997) were employed to solve for the eigenvalues and eigenvectors.

2.4 DMS and intensities

Intensity computation requires high-quality electric DMS. We use an ab initio DMS computed at the CCSD(T)/aug-cc-pVQZ level of theory in the frozen-core approximation using CFOUR (Harding et al. 2008). Three symmetry-adapted projections of the dipole moment Cartesian components, $\mu_{\rm A_1}$, $\mu_{\rm B_1}$ and $\mu_{\rm B_2}$, are given in the analytical representations with each component expanded in Taylor series (185 parameters in total) in terms of internal coordinates around the equilibrium configuration using the form developed by Yachmenev, Polyak & Thiel (2013) to represent the dipole moment of H_2CS. These parameters reproduce the ab initio dipole moment values of the $\mu_{\rm A_1}$, $\mu_{\rm B_1}$ and $\mu_{\rm B_2}$ components with rms errors of 0.0002 D for each component. The equilibrium value of our dipole moment is 2.3778 D (at $r^{\rm e}_{\rm CO} = 1.203\ 3742$ Å, $r^{\rm e}_{\rm CH} = 1.103\ 77$ Å, $\theta^{\rm e}_{\rm OCH} = 121.844^\circ$), which can be compared to the experimental value of the ground vibrational state dipole moment of $\mu = 2.3321(5)$ D measured by Fabricant, Krieger & Muenter (1977).

The eigenvectors, obtained by diagonalization, are used in conjunction with the DMS to compute the required line strengths (and from that the Einstein-A coefficients and absolute intensities) of transitions that satisfy the rotational selection rules

$$J' - J'' = 0, \pm 1, \ J' + J'' \neq 0 \tag{6}$$

and the symmetry selection rules

$$A_1 \leftrightarrow A_2 \ , B_1 \leftrightarrow B_2. \tag{7}$$

The Einstein-A coefficient for a particular transition from the *initial* state i to the *final* state f is given by

$$A_{if} = \frac{8\pi^4 \tilde{\nu}_{if}^3}{3h}(2J_i + 1) \sum_{A=X,Y,Z} |\langle \Psi^f | \bar{\mu}_A | \Psi^i \rangle|^2, \tag{8}$$

where J_i is the rotational quantum number for the initial state, h is the Planck constant, $\tilde{\nu}_{if}$ is the transition frequency ($hc\,\tilde{\nu}_{if} = E_f - E_i$),

Table 2. Extract from the H_2CO state file. The full table is available at http://cdsarc.u-strasbg.fr/cgi-bin/VizieR?-source=J/MNRAS/.

I	$\tilde{E}$ (cm^{-1})	g	J	$\Gamma_{\rm tot}$	v_1	v_2	v_3	v_4	v_5	v_6	$\Gamma_{\rm vib}$	K	$\Gamma_{\rm rot}$	$I_{J,\Gamma}$	$\lvert C_i^2\rvert$	n_1	n_2	n_3	n_4	n_5	n_6
1	0.000 000	1	0	1	0	0	0	0	0	0	1	0	1	1	0.99	0	0	0	0	0	0
2	1500.120 955	1	0	1	0	0	1	0	0	0	1	0	1	2	0.92	0	0	0	0	1	0
3	1746.045 388	1	0	1	0	1	0	0	0	0	1	0	1	3	0.92	1	0	0	0	0	0
4	2327.497 142	1	0	1	0	0	0	2	0	0	1	0	1	4	0.97	0	0	0	0	0	2
5	2494.322 937	1	0	1	0	0	0	0	0	2	1	0	1	5	0.96	0	0	0	1	1	0
6	2782.410 921	1	0	1	1	0	0	0	0	0	1	0	1	6	0.97	0	0	1	0	0	0
7	2999.006 647	1	0	1	0	0	2	0	0	0	1	0	1	7	0.84	0	0	0	1	1	0
8	3238.937 891	1	0	1	0	1	1	0	0	0	1	0	1	8	0.70	1	0	0	0	1	0
9	3471.719 306	1	0	1	0	2	0	0	0	0	1	0	1	9	0.83	2	0	0	0	0	0
10	3825.967 015	1	0	1	0	0	1	2	0	0	1	0	1	10	0.86	0	0	0	0	1	2
11	3936.435 541	1	0	1	0	0	1	0	0	2	1	0	1	11	0.73	0	0	0	3	0	0
12	4058.101 422	1	0	1	0	1	0	2	0	0	1	0	1	12	0.87	1	0	0	0	0	2
13	4083.490 190	1	0	1	0	0	0	0	1	1	1	0	1	13	0.69	0	1	0	1	0	0
14	4247.609 826	1	0	1	0	1	0	0	0	2	1	0	1	14	0.79	1	0	0	1	1	0
15	4256.314 862	1	0	1	1	0	1	0	0	0	1	0	1	15	0.90	0	0	1	0	1	0
16	4495.499 848	1	0	1	0	0	3	0	0	0	1	0	1	16	0.76	0	0	0	1	2	0
17	4529.635 737	1	0	1	1	1	0	0	0	0	1	0	1	17	0.90	1	0	1	0	0	0

Notes. I: State counting number;
$\tilde{E}$: state term energy in cm^{-1};
g: state degeneracy;
J: state rotational quantum number;
$\Gamma_{\rm tot}$: total symmetry in $C_{2v}(M)$ (1 is A_1, 2 is A_2, 3 is B_1 and 4 is B_2);
$v_1 - v_6$: normal mode vibrational quantum numbers;
$\Gamma_{\rm vib}$: symmetry of vibrational contribution in $C_{2v}(M)$;
K: state projection of the rotational quantum number;
$\Gamma_{\rm rot}$: symmetry of rotational contribution in $C_{2v}(M)$;
$I_{J,\Gamma}$: state number in J, Γ block;
$|C_i^2|$: largest coefficient used in the assignment;
$n_1 - n_6$: TROVE vibrational quantum numbers.

Ψ^f and Ψ^i represent the eigenfunctions of the final and initial states, respectively, and $\bar{\mu}_A$ is the electronically averaged component of the dipole moment along the space-fixed axis $A = X, Y, Z$ (see also Yurchenko et al. 2005a). From this the absolute absorption intensity is determined by

$$I(f \leftarrow i) = \frac{A_{if}}{8\pi c} g_{\rm ns}(2J_f+1)\frac{\exp\left(-\frac{E_i}{kT}\right)}{Q\ \tilde{\nu}_{if}^2}\left[1-\exp\left(\frac{-hc\tilde{\nu}_{if}}{kT}\right)\right], \quad (9)$$

where k is the Boltzmann constant, T is the absolute temperature and $g_{\rm ns}$ is the nuclear spin statistical weight factor. Q, the partition function, is given by

$$Q = \sum_i g_i \exp\left(\frac{-E_i}{kT}\right), \quad (10)$$

where g_i is the degeneracy of a particular state i with energy E_i. For H_2CO, g_i is $g_{\rm ns}(2J_i + 1)$ with $g_{\rm ns} = 1$ for A_1 and A_2 symmetries and $g_{\rm ns} = 3$ for B_1 and B_2 symmetries. The transitions were computed using the energy limits hc 8000 and hc 18 000 cm^{-1} for the lower and upper states, respectively.

Although diagonalization of the Hamiltonian matrices is very demanding on computer resources, it is the calculation of the Einstein-A coefficients which dominates the actual computer time due to the sheer number of these and the large size of the eigenvectors. Graphics processing units were therefore employed to accelerate computation of the intensities. To do this required the development of a new algorithm to allow these fast but memory-poor processors to be used efficiently. A paper discussing this will be published elsewhere (Al-Refaie, Tennyson & Yurchenko 2015).

3 RESULTS

The line list produced, which we call AYTY, contains around 10 billion transitions with wavenumbers up to 10 000 cm^{-1}. The transitions are sorted in increasing transition frequency and then converted into the ExoMol format (Tennyson, Hill & Yurchenko 2013). An extract of the state file and transition file can be seen in Tables 2 and 3. Spectra at arbitrary temperatures can be computed using the Einstein-A coefficients from the transition files. The theoretical error is estimated by the fitting rms deviation of 0.18 cm^{-1}. This means our transition frequencies and energy levels should be reliable to about 0.2 cm^{-1} with low-lying levels, particularly the pure rotational ones, being much more accurate than this and levels for vibrational states for which there are no available laboratory data much less so.

Table 3. Extracts from the H_2CO transition file. The full table is available at http://cdsarc.u-strasbg.fr/cgi-bin/VizieR?-source=J/MNRAS/

f	i	A_{fi}
6713 828	6734 990	8.2910e−06
6709 468	6722 660	3.2621e−05
6704 996	6726 710	4.7333e−05
6726 711	6739 070	5.0697e−05
6718 218	6730 865	5.4273e−05
6730 866	6750 469	5.6752e−05

Notes. f: Upper state counting number; i: lower state counting number; A_{fi}: Einstein-A coefficient in s^{-1}.

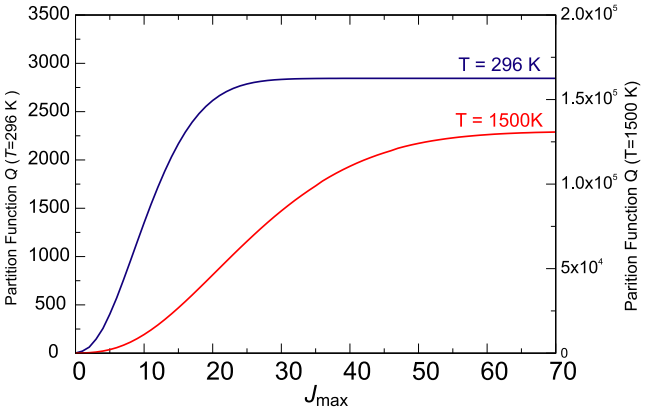

Figure 2. Partition functions at two temperatures as a function of inclusion of rotational states: all J up to $J_{\rm max}$ for $T = 296$ K (left-hand scale) and $T = 1500$ K (right-hand scale).

The completeness of the line list as a function of temperature can be determined by checking the convergence of the temperature-dependent partition function Q given in equation (10), which is computed via explicit summation (Vidler & Tennyson 2000) of the 10.3 million energy levels available. As T increases, a greater proportion of these states are required as their contribution towards Q becomes more important. Fig. 2 shows our computed partition function as a function of the maximum J value ($J_{\rm max}$) used in the calculation. As $J_{\rm max}$ increases, each J contributes progressively less until convergence is reached. The partition function at $T = 296$ K converges to better than 1 per cent at $J \approx 34$ with the limit of $Q = 2844.621$ at $J = 58$. For =1500 K, it converges to about 0.005 per cent at $J = 70$ with a Q value of 130 190.25. These partition functions can be used to evaluate the effect of lower energy state threshold of 8000 cm^{-1} on the completeness of the line list by comparing $Q_{\rm limit}$, which sums energies up to this threshold, with the full partition sum. Fig. 3 shows that the two partition functions are essentially the same up to 800 K and that $Q_{\rm limit}$ is 92.3 per cent of Q at $T = 1500$ K. Therefore, we recommend $T = 1500$ K as a 'soft' limit to the applicability of the line list. Use of the line list at higher temperatures will lead to the progressive loss of opacity although the ratio $Q_{\rm limit}/Q$ can be used to estimate the proportion of this missing contribution (Neale, Miller & Tennyson 1996).

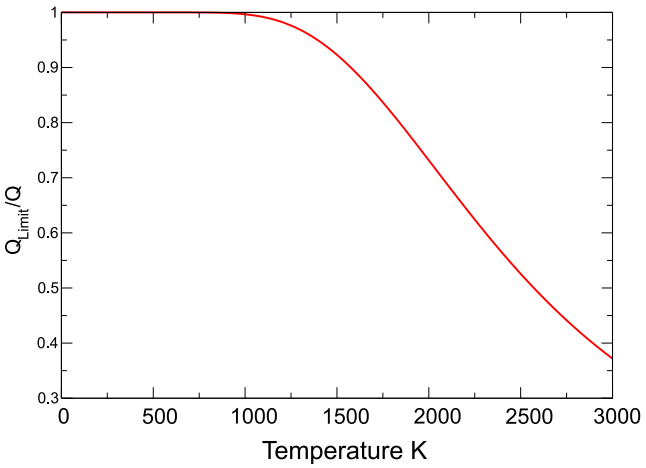

Figure 3. Plot of $Q_{\rm limit}/Q$ against temperature, where $Q_{\rm limit}$ is the partition function computed using only energy levels below our lower state threshold of 8000 cm^{-1}.

Table 4. Comparisons of H_2CO partition functions as a function of temperature for this work, CDMS (Müller et al. 2005) and those used in HITRAN (Fischer et al. 2003).

T (K)	AYTY	CDMS	HITRAN
2.725	2.0165	2.0166	
5.000	4.4833	4.4832	
9.375	13.801	13.8008	
18.75	44.6835	44.6812	
37.5	128.6581	128.6492	
75	361.7053	361.7195	362.07
150	1019.9549	1019.9706	1020.47
225	1874.4679	1872.6221	1875.67
300	2904.1778	2883.0163	2906.32
500	6760.2315	6208.3442	6760.99
1500	128 635.40		130 190.25
3000	2741 283.3		3038 800.0

Table 5. Parameters used to represent the partition function, see equation (11), valid for temperatures up to 3000 K.

Parameter	Value
a_0	1.127 898 076 83
a_1	−5.350 679 398 66
a_2	10.336 843 237 00
a_3	−4.921 874 551 47
a_4	−2.282 340 893 65
a_5	3.611 228 217 99
a_6	−1.641 743 653 25
a_7	0.337 275 432 06
a_8	−0.026 542 231 36

Table 4 compares our partition functions with those from CDMS (Müller et al. 2005) and those used in HITRAN (Fischer et al. 2003). At temperatures $T \leq 300$ K, we agree to better than 1 per cent with CDMS and HITRAN. At 500 K the difference with CDMS is much higher at 8.9 per cent, due to our explicit sum running over a much larger number of levels, but agreement with HITRAN is good. There are bigger differences at higher temperatures: at 1500 K our partition function is lower by about 1.2 per cent and at 3000 K by 9.7 per cent. This may be caused by the lack of the high-energy contributions due to the energy cut-off of hc 18 000 cm^{-1} used in our line list, see Sousa-Silva et al. (2014) and Neale & Tennyson (1995) for a discussion of the importance of contributions from the excited ro-vibrational states up to the dissociation. Our full partition function evaluated on a 1 K grid is given in the supplementary data.

We use the analytical representation suggested by Vidler & Tennyson (2000) as given by

$$\log_{10} Q(T) = \sum_{n=0}^{8} a_n \left[\log_{10} T\right]^n . \quad (11)$$

The expansion parameters given in Table 5 reproduce our partition function better than 0.3 per cent for temperatures ranging up to 3000 K.

The dependence of the cross-sections on temperature is illustrated in Fig. 4; the features in the simulated spectra become smoother as the temperature increases. This is a result of the vibrationally excited states becoming more populated and the increasing width of the rotational envelope with temperature. Fig. 5 shows a simulated $T = 296$ K spectrum computed from our line list against the available laboratory absorption spectra up to 10 000 cm^{-1}.The logarithmic scale used shows the density of transitions in our line list and reveals the significant gaps and limitations in the HITRAN 2012 data base. Comparing specific regions, our line list accurately replicates both the line positions and intensities of the three available bands, as illustrated in detail in Fig. 6. Additional lines are present as our computed spectra contain all possible transitions within the region including hot bands. Fig. 6(d) and Table 6 show agreement with the line positions and absolute intensities from Reuter et al. (1989) with an rms deviation of 0.099 cm^{-1} for the line positions. There are some limitations with our line list. Higher J transitions at around the $J > 50$ range begin to show a slight drift of ≈0.3 cm^{-1} in the predicted line position; this does not occur for the rotational band. In practice, errors in the ro-vibrational energy levels grow with K (as

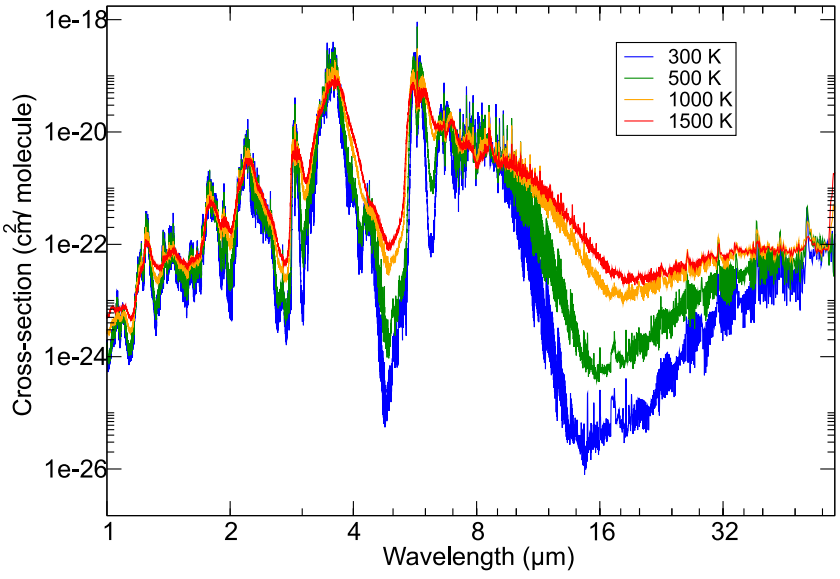

Figure 4. Cross-sections of the entire AYTY line list as a function of temperature. The curves in the 16 μm region increase in opacity with the increase in temperature.

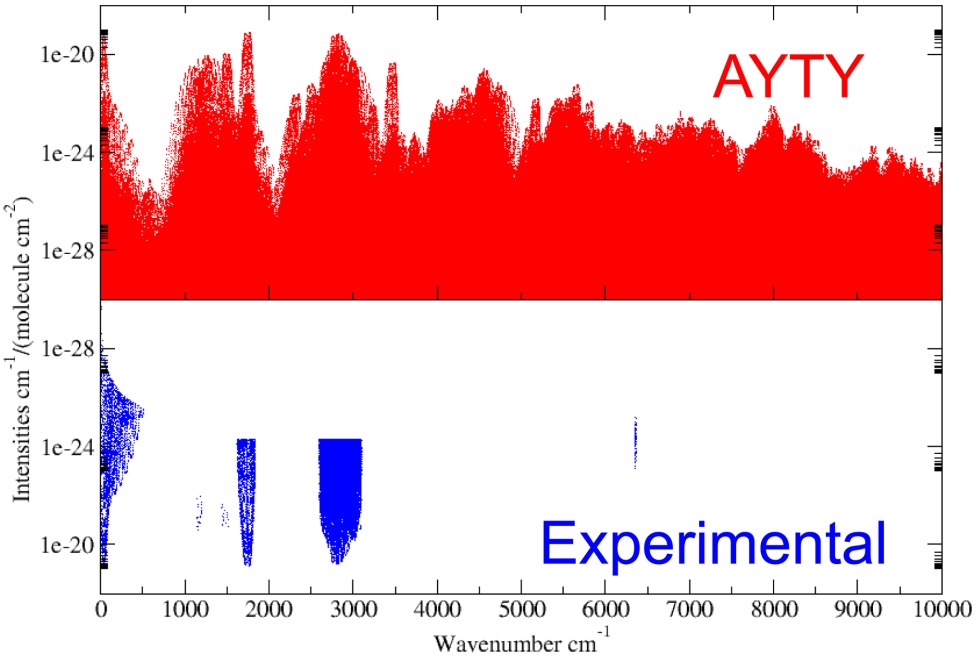

Figure 5. Overview of our synthetic spectrum at $T = 296$ K against HITRAN (Rothman et al. 2013), Reuter et al. (1989) and Zhao et al. (2007).

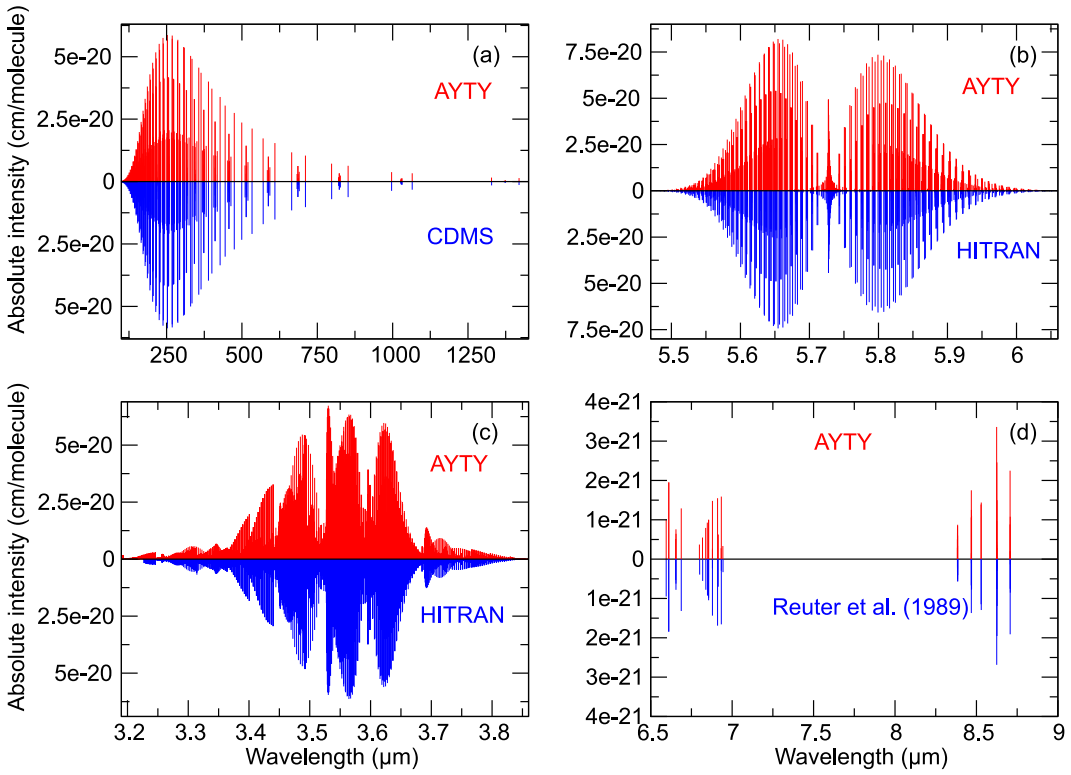

Figure 6. The fundamental bands compared to currently available experimental intensities (Reuter et al. 1989; Müller et al. 2005; Rothman et al. 2013) at $T = 296$ K. (a) Rotational band; (b) ν_2; (c) ν_1 and ν_5; (d) ν_3, ν_4 and ν_6.

opposed to J); the discrepancies in transition frequencies become more pronounced in $|K' - K''| = 1$ transitions than those that involve the same K ($K' = K''$). This can be seen in the lack of drift in the pure rotational band as it is mostly comprised of $K' = K''$ transitions due to both ground and excited states being of A_1 symmetry. B_1 and B_2 vibrational bands however are mostly comprised of $|K' - K''| = 1$ transitions which makes their errors more sensitive to the quality of the model.

Computing band intensities requires simulating spectra at a chosen temperature and accumulating all transitions that correspond to the specific band. Table 7 highlights our band intensities against those available in the literature. Each band intensity required

Table 6. Residuals, in cm^{-1}, for line positions for the ν_3, ν_4 and ν_6 bands. Observed data from Reuter et al. (1989).

Band	J'	J''	AYTY	Obs.	Obs.−Calc.
6	17	18	1148.4322	1148.3346	−0.0976
6	17	18	1148.4578	1148.3600	−0.0978
4	11	10	1148.4115	1148.3453	−0.0662
4	3	4	1148.5548	1148.4702	−0.0846
4	16	16	1148.6150	1148.5082	−0.1068
4	1	1	1159.2222	1159.1356	−0.0866
4	2	2	1159.3587	1159.2716	−0.0871
4	28	28	1159.3222	1159.3070	−0.0152
4	15	14	1159.4760	1159.3917	−0.0843
6	6	7	1159.5539	1159.4132	−0.1407
4	9	8	1159.5115	1159.4396	−0.0719
4	3	3	1159.5594	1159.4715	−0.0879
4	18	18	1172.4242	1172.3864	−0.0378
4	6	6	1172.6002	1172.5256	−0.0746
6	12	13	1180.6607	1180.6446	−0.0161
6	4	5	1180.8080	1180.7328	−0.0752
4	24	23	1180.8209	1180.8082	−0.0127
4	11	11	1180.8777	1180.8324	−0.0453
6	13	14	1180.9109	1180.8834	−0.0275
6	10	10	1192.6923	1192.6086	−0.0837
6	3	4	1192.6678	1192.6267	−0.0411
6	9	9	1192.7477	1192.6657	−0.0820
6	8	8	1192.7985	1192.7181	−0.0804
6	18	19	1192.7781	1192.7369	−0.0412
6	7	7	1192.8441	1192.7651	−0.0790
6	10	11	1192.7723	1192.7954	0.0231
6	6	6	1192.8845	1192.8067	−0.0778
6	5	5	1192.9194	1192.8427	−0.0767
6	19	18	1440.3351	1440.1330	−0.2021
6	20	19	1442.4701	1442.2633	−0.2068
6	17	16	1460.4035	1460.1831	−0.2204
6	18	17	1462.5117	1462.2863	−0.2254
6	20	19	1466.6771	1466.4415	−0.2356
6	22	21	1470.7763	1470.5289	−0.2474
3	24	25	1442.2597	1442.2329	−0.0268
3	22	23	1446.1622	1446.2088	0.0466
3	22	23	1447.1125	1447.1250	0.0125
3	19	20	1453.7010	1453.7073	0.0063
3	20	21	1453.7236	1453.7154	−0.0082
3	17	18	1458.7043	1458.7231	0.0188
3	17	18	1458.7141	1458.7325	0.0184
3	1	2	1495.2715	1495.3254	0.0539
3	1	0	1502.5583	1502.6118	0.0535
3	9	9	1502.6600	1502.6548	−0.0052
3	11	11	1502.9248	1502.9188	−0.0060
3	5	4	1512.6148	1512.6595	0.0447
3	5	4	1512.6741	1512.7189	0.0448
3	6	5	1516.3213	1516.3326	0.0113

spectra simulated to the parameters used by each reference. In general, AYTY agrees well with all band intensities but is more intense. This may be due to the fact that AYTY sums over all lines in a given band whereas experiments generally only capture the strongest lines. Table 7 also shows the total band intensity for the 3.5 μm region compared to that by Brown et al. (1979), Nakanaga et al. (1982) and HITRAN. Our value is 13 per cent stronger than HITRAN (matches the discrepancy for the ν_1 and ν_5 bands in Table 7), 18 per cent stronger than Nakanaga et al. (1982) and 40 per cent stronger than that by Brown et al. (1979). Absolute intensities and bands not available in the HITRAN data base or literature can be evaluated against cross-sections. For the ν_3, ν_4 and ν_6 bands, further evaluation of these bands can be made against cross-sections available from the PNNL-IR data base (Sharpe et al. 2004) and Nakanaga et al. (1982) using a Gaussian profile with an HWHM (half-width at half-maximum) of 1.1849 and 0.1120 cm^{-1}, determined from their respective experimental profiles. Fig. 7(a) compares the AYTY line list with a spectrum extracted from fig. 3 of Nakanaga et al. (1982) and scaled to match the AYTY line list. Good agreement is seen in both structure and position in the band with a slight drift occurring as an artefact from the extraction process. Fig. 7(b) shows even better agreement with the spectral structure as well as the cross-section intensity.

Table 7. Band intensities, in 10^{-17} cm^{-1}/(molecule cm^{-2}).

Band	Ref.	Obs	AYTY	(O−A)/O (per cent)
ν_1	[a]	1.008	1.057	−4.9
ν_2	[a]	1.219	1.348	−10.6
ν_3	[b]	0.184	0.185	−0.5
ν_4	[b]	0.069	0.089	−27.8
ν_5	[a]	1.120	1.282	−14.6
ν_6	[a]	0.173	0.204	−17.9
$\nu_2+\nu_3$	[c]	0.0025	0.0019	22.7
$\nu_2+\nu_6$	[c]	0.0790	0.1222	−54.6
$2\nu_3$	[c]	0.0260	0.0428	−64.5
$\nu_2+\nu_4$	[c]	0.1100	0.1379	−25.4
$\nu_3+\nu_6$	[c]	0.1940	0.3274	−68.8
$\nu_3+\nu_4$	[c]	0.0290	0.0300	−3.4
$2\nu_6$	[c]	0.0220	0.0214	2.9
$\nu_4+\nu_6$	[c]	0.0062	0.0014	77.7
$2\nu_4$	[c]	0.0060	0.0047	22.4
$\nu_1+\nu_6$	[d]	0.0015	0.0022	−45.0
$\nu_2+\nu_4+\nu_6$	[d]	0.0006	0.0007	−4.6
$\nu_3+\nu_5$	[d]	0.0097	0.0098	−1.2
$2\nu_3+\nu_6$	[d]	0.0036	0.0027	24.4
$\nu_2+\nu_5$	[d]	0.0377	0.0446	−18.2
$2\nu_2+\nu_6$	[d]	0.0108	0.0123	−14.0
$\nu_1+\nu_2$	[d]	0.0243	0.0275	−13.2
$3\nu_2$	[d]	0.0022	0.0026	−21.4

Notes. [a]Perrin et al. (2009); [b]Perrin et al. (2003); [c]Perrin et al. (2006); [d]Flaud et al. (2006).

The total integrated cross-section over the region 6.2–10.5 μm for AYTY and PNNL is 8.02×10^{-17} and 8.20×10^{-17} cm per molecule, respectively, making PNNL overall around 8 per cent stronger. PNNL covers regions beyond those currently available in HITRAN. Fig. 8(a) depicts the $2\nu_2$ band at 2.88 μm. Good agreement is seen in structure, position and cross-sections with the integrated cross-sections differing by only 10 per cent. The regions below 2.8 μmin PNNL become increasingly polluted with noise but band features are still visible as seen in Figs 8(b)–(d). In particular, as shown in Fig. 8(b), the AYTY cross-section reproduces peaks in features present in the PNNL-IR data. This region was also studied by Flaud et al. (2006). Their absorbance spectrum produces certain transitions with double the intensity compared to AYTY. These are due to splitting caused by two transitions with the same quanta but with swapped Γ_f and Γ_i giving the two lines very similar transition frequencies and absolute intensity which make them difficult to resolve experimentally.

Further bands include the integrated cross-section for the $2\nu_5$ band at 5676.21 cm^{-1} for AYTY and Barry et al. (2002) at 6.4×10^{-22} and 5.6×10^{-22} cm per molecule, respectively, making AYTY 11 per cent stronger. In Table 7 we also compare theoretical (AYTY) overtone band intensities obtained by the direct summation

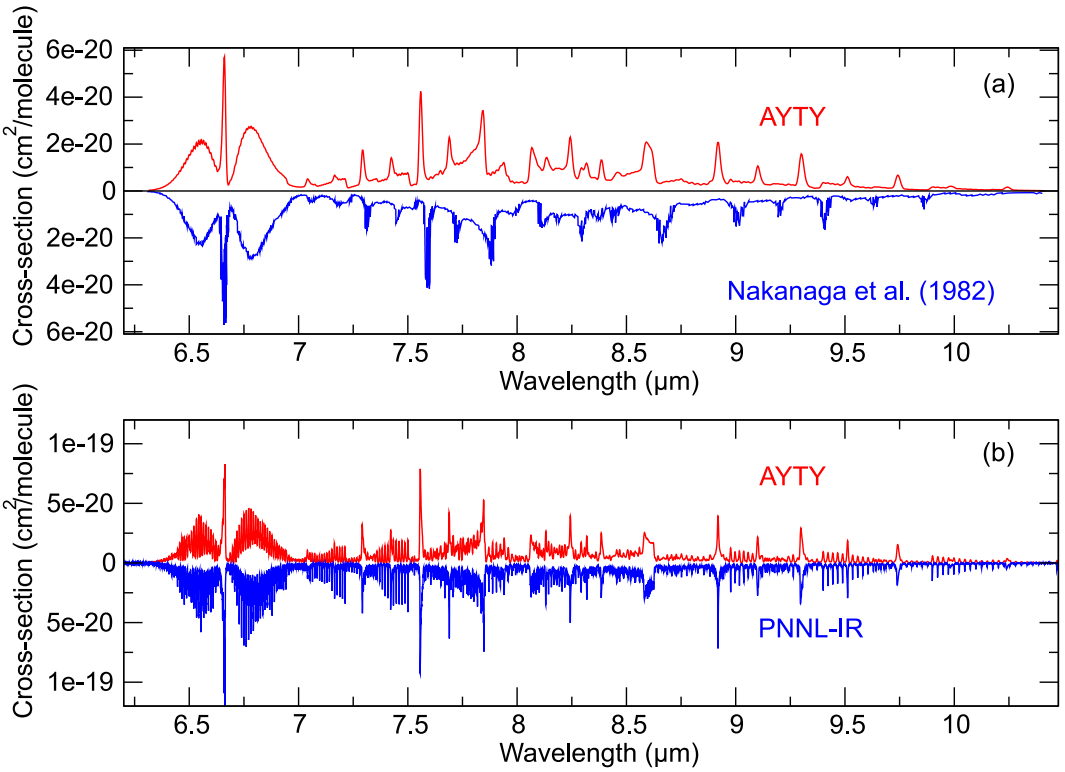

Figure 7. Cross-section comparison of AYTY against experimental of the ν_3, ν_4 and ν_6 band regions: (a) Nakanaga et al. (1982) at 296 K with HWHM = 1.1849 cm^{-1}; extracted from image and scaled to match the AYTY cross-section; (b) PNNL-IR data at 323.15 K (Sharpe et al. 2004) with HWHM = 0.1120 cm^{-1}.

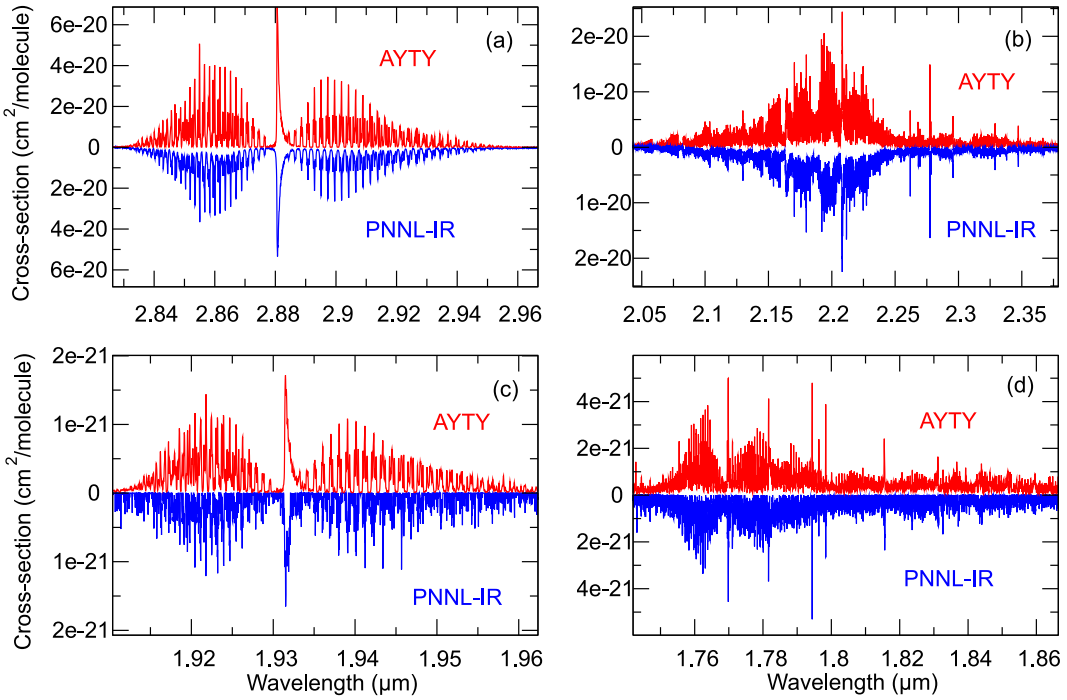

Figure 8. Additional bands in PNNL at wavelengths below 3.2 μm with HWHM at 0.1120 cm^{-1}. (a) $2\nu_2$ band; (b) bands covered by Flaud et al. (2006); (c) $3\nu_2$; (d) various bands including $\nu_1 + \nu_5$. Note: (c) and (d) negative PNNL values have been removed.

with the corresponding experimentally derived values from Perrin et al. (2006) and Flaud et al. (2006). The agreement with the data obtained by Flaud et al. (2006) is very good. Those from Perrin et al. (2006) are in fact a compilation of different sources (Hisatsune & Eggers 1955; Brown et al. 1979; Nakanaga et al. 1982; Cline & Varghese 1988; Herndon et al. 2005), some of which were obtained at low resolution, which could explain the slightly worse agreement with our calculations. Comparing the total integrated band intensity for the band at 1.5 μm, we obtain 3.11×10^{-17} cm per molecule against 2.19, 2.62 and 2.73×10^{-17} cm per molecule by Perrin et al. (2006), Nakanaga et al. (1982) and from HITRAN, respectively.

Finally, Ito et al. (1994) presented the relative band intensities as the ratio of the vibrational transition moments between $2\nu_4$ and $2\nu_6$ of 0.755(48), which can be compared to our absolute value of 0.6264.

4 CONCLUSION

We have computed the frequency and Einstein-*A* coefficients of almost 10 billion transitions of formaldehyde, which cover wavelengths longer than 1 μm and include all rotational excitations up to $J = 70$, making the line list applicable for temperatures up to 1500 K. The AYTY line list gives a room-temperature spectrum in excellent agreement with available experimental data. We have highlighted those regions missing from the HITRAN data base with the hope that they will be investigated further experimentally. The new line list may be accessed via www.exomol.com or http://cdsarc.u-strasbg.fr/viz-bin/qcat?J/MNRAS/. The cross-sections of H_2CO can also be generated at www.exomol.com as described by Hill, Yurchenko & Tennyson (2013).

ACKNOWLEDGEMENTS

This work was supported by the ERC under the Advanced Investigator Project 267219 and made use of the DiRAC@Darwin, DiRAC@COSMOS HPC cluster and Emerald CfI cluster. DiRAC is the UK HPC facility for particle physics, astrophysics and cosmology and is supported by STFC and BIS. The authors would like to acknowledge that the work presented here made use of the EMERALD High Performance Computing facility provided via the Centre for Innovation (CfI). The CfI is formed from the universities of Bristol, Oxford, Southampton and UCL in partnership with STFC Rutherford Appleton Laboratory. The authors would like to thank Clara Sousa-Silva and Duncan A. Little for help during the writing of this paper. AFA would also like to thank Dr Faris N. Al-Refaie, Lamya Ali, Sarfraz Ahmed Aziz, Rory Gleeson and Annie Gleeson for their support.

REFERENCES

Al-Refaie A. F., Tennyson J., Yurchenko S. N., 2015, Comput. Phys. Commun., submitted
Anderson E. et al., 1999, LAPACK Users' Guide, 3rd edn. SIAM, Philadelphia, PA
Araya E., Hofner P., Sewio M., Linz H., Kurtz S., Olmi L., Watson C., Churchwell E., 2007, ApJ, 654, L95
Barry H., Corner L., Hancock G., Peverall R., Ritchie G. A. D., 2002, Phys. Chem. Chem. Phys., 4, 445
Blackford L. S. et al., 1997, ScaLAPACK Users' Guide. SIAM, Philadelphia, PA
Bockelee-Morvan D., Crovisier J., 1992, A&A, 264, 282
Brown L. R., Hunt R. H., Pine A. S., 1979, J. Mol. Spectrosc., 75, 406
Bunker P. R., Jensen P., 1998, Molecular Symmetry and Spectroscopy, 2nd edn. NRC Research Press, Ottawa
Carter S., Pinnavaia N., Handy N. C., 1995, Chem. Phys. Lett., 240, 400
Carter S., Sharma A. R., Bowman J. M., Rosmus P., Tarroni R., 2009, J. Chem. Phys., 131, 224106
Cline D. S., Varghese P. L., 1988, Appl. Opt., 27, 3219
Clouthier D. J., Ramsay D. A., 1983, Annu. Rev. Phys. Chem., 34, 31
Cooley J. W., 1961, Math. Comp., 15, 363
Cottin H., Gazeau M. C., Benilan Y., Raulin F., 2001, ApJ, 556, 417
Dello Russo N. et al., 2011, ApJ, 734, L8
Eckart C., 1935, Phys. Rev., 47, 552
Fabricant B., Krieger D., Muenter J. S., 1977, J. Chem. Phys., 67, 1576
Fischer J., Gamache R. R., Goldman A., Rothman L. S., Perrin A., 2003, J. Quant. Spectrosc. Radiat. Transfer, 82, 401
Flaud J. M., Lafferty W. J., Sams R. L., Sharpe S. W., 2006, Mol. Phys., 104, 1891
Forster J. R., Goss W. M., Wilson T. L., Downes D., Dickel H. R., 1980, A&A, 84, L1
Goldman N., Tamblyn I., 2013, J. Phys. Chem. A, 117, 5124
Harding M. E., Metzroth T., Gauss J., Auer A. A., 2008, J. Chem. Theory Comput., 4, 64
Herndon S., Nelson D., Li Y., Zahniser M., 2005, J. Quant. Spectrosc. Radiat. Transfer, 90, 207
Hill C., Yurchenko S. N., Tennyson J., 2013, Icarus, 226, 1673
Hisatsune I. C., Eggers D. F., 1955, J. Chem. Phys., 23, 487
Hollis J. M., Lovas F. J., Jewell P. R., 2000, ApJ, 540, L107
Ito F., Nakanaga T., Takeo H., 1994, Spectrochim. Acta A, 50, 1397
Johns J. W. C., McKellar A. R. W., 1975, J. Chem. Phys., 63, 1682
Korablev O. I., Ackerman M., Krasnopolsky V. A., Moroz V. I., Muller C., Rodin A. V., Aterya S. K., 1993, Planet. Space Sci., 41, 441
Kozin I. N., Law M. M., Tennyson J., Hutson J. M., 2004, Comput. Phys. Commun., 163, 117
Langer W. D., 1976, ApJ, 210, 328
Luckhaus D., Coffey M. J., Fritz M. D., Crim F. F., 1996, J. Chem. Phys., 104, 3472
Mangum J. G., Darling J., Menten K. M., Henkel C., 2008, ApJ, 673, 832
Margules L., Perrin A., Janeckova R., Bailleux S., Endres C. P., Giesen T. F., Schlemmer S., 2009, Can. J. Phys., 87, 425
Milam S. N. et al., 2006, ApJ, 649, 1169
Müller H. S. P., Schlöder F., Stutzki J., Winnewisser G., 2005, J. Mol. Struct., 742, 215
Nadler S., Daunt S. J., Reuter D. C., 1987, Appl. Opt., 26, 1641
Nakagawa T., Morino Y., 1971, J. Mol. Spectrosc., 38, 84
Nakanaga T., Kondo S., Saeki S., 1982, J. Chem. Phys., 76, 3860
Neale L., Tennyson J., 1995, ApJ, 454, L169
Neale L., Miller S., Tennyson J., 1996, ApJ, 464, 516
Neveu M., Kim H.-J., Benner S. A., 2013, Astrobiology, 13, 391
Noumerov B. V., 1924, MNRAS, 84, 592
Öberg K. I. et al., 2010, ApJ, 720, 480
Perez R., Brown J. M., Utkin Y., Han J. X., Curl R. F., 2006, J. Mol. Spectrosc., 236, 151
Perrin A., Keller F., Flaud J. M., 2003, J. Mol. Spectrosc., 221, 192
Perrin A., Valentin A., Daumont L., 2006, J. Mol. Struct., 780, 28
Perrin A., Jacquemart D., Tchana F. K., Lacome N., 2009, J. Quant. Spectrosc. Radiat. Transfer, 110, 700
Polyansky O. L., Kozin I. N., Maĺyszek P., Koput J., Tennyson J., Yurchenko S. N., 2013, J. Phys. Chem. A, 117, 7367
Poulin N. M., Bramley M. J., Carrington T., Kjaergaard H. G., Henry B. R., 1996, J. Chem. Phys., 104, 7807
Pratap P., Snyder L. E., Batrla W., 1992, ApJ, 387, 241
Reuter D. C., Nadler S., Daunt S. J., Johns J. W. C., 1989, J. Chem. Phys., 91, 646
Rothman L. S. et al., 2009, J. Quant. Spectrosc. Radiat. Transfer, 110, 533
Rothman L. S. et al., 2013, J. Quant. Spectrosc. Radiat. Transfer, 130, 4
Sargent B. A. et al., 2014, ApJ, 792, 83
Schutte W. A., 2002, Adv. Space Res., 30, 1409
Sharpe S. W., Johnson T. J., Sams R. L., Chu P. M., Rhoderick G. C., Johnson P. A., 2004, Appl. Spectrosc., 58, 1452

Sousa-Silva C., Yurchenko S. N., Tennyson J., 2013, J. Mol. Spectrosc., 288, 28
Sousa-Silva C., Hesketh N., Yurchenko S. N., Hill C., Tennyson J., 2014, J. Quant. Spectrosc. Radiat. Transfer, 142, 66
Sousa-Silva C., Al-Refaie A. F., Tennyson J., Yurchenko S. N., 2015, MNRAS, 446, 2337
Tchana F. K., Perrin A., Lacome N., 2007, J. Mol. Spectrosc., 245, 141
Tennyson J., Yurchenko S. N., 2012, MNRAS, 425, 21
Tennyson J., Hill C., Yurchenko S. N., 2013, in Gillaspy J. D., Wiese W. L., Podpaly Y. A., eds, AIP Conf. Proc. Vol. 1545, 8th International Conference on Atomic and Molecular Data and Their Applications ICAMDATA-2012. Am. Inst. Phys., New York, p. 186
Theulé P., Callegari A., Rizzo T. R., Muenter J. S., 2003, J. Chem. Phys., 119, 8910
Underwood D. S., Tennyson J., Yurchenko S. N., 2013, Phys. Chem. Chem. Phys., 15, 10118
Vidler M., Tennyson J., 2000, J. Chem. Phys., 113, 9766
Villanueva G. L., Mumma M. J., Disanti M. A., Bonev B. P., Gibb E. L., Magee-Sauer K., Blake G. A., Salyk C., 2011, Icarus, 216, 227
Villanueva G. et al., 2013, Icarus, 223, 11
Wayne R. P., 2000, Chemistry of Atmospheres. Oxford Univ. Press, Oxford
Woon D. E., 2002, ApJ, 569, 541
Yachmenev A., Yurchenko S. N., Jensen P., Baum O., Giesen T. F., Thiel W., 2010, Phys. Chem. Chem. Phys., 12, 8387
Yachmenev A., Yurchenko S. N., Jensen P., Thiel W., 2011, J. Chem. Phys., 134, 11
Yachmenev A., Polyak I., Thiel W., 2013, J. Chem. Phys., 139, 204308
Yurchenko S. N., 2014, in Springborg M., Joswig J.-O., eds, Chemical Modelling: Volume 10. Royal Society of Chemistry, Cambridge, p. 183
Yurchenko S. N., Tennyson J., 2014, MNRAS, 440, 1649
Yurchenko S. N., Thiel W., Carvajal M., Lin H., Jensen P., 2005a, Adv. Quantum Chem., 48, 209
Yurchenko S. N., Carvajal M., Jensen P., Lin H., Zheng J. J., Thiel W., 2005b, Mol. Phys., 103, 359
Yurchenko S. N., Thiel W., Jensen P., 2007, J. Mol. Spectrosc., 245, 126
Yurchenko S. N., Barber R. J., Yachmenev A., Thiel W., Jensen P., Tennyson J., 2009, J. Phys. Chem. A, 113, 11845
Yurchenko S. N., Carvajal M., Yachmenev A., Thiel W., Jensen P., 2010, J. Quant. Spectrosc. Radiat. Transfer, 111, 2279
Yurchenko S. N., Barber R. J., Tennyson J., 2011, MNRAS, 413, 1828
Zasowski G., Kemper F., Watson D. M., Furlan E., Bohac C. J., Hull C., Green J. D., 2009, ApJ, 694, 459
Zhao W., Gao X., Deng L., Huang T., Wu T., Zhang W., 2007, J. Quant. Spectrosc. Radiat. Transfer, 107, 331
Zuckerman B., Buhl D., Palmer P., Snyder L. E., 1970, ApJ, 160, 485
Zuckerman B., Buhl D., Palmer P., Snyder L. E., 1974, ApJ, 189, 217

SUPPORTING INFORMATION

Additional Supporting Information may be found in the online version of this article:

H2CO_AYTY.pf
H2CO_DMS_2014.f90
H2CO_DMS_2014.inp
H2CO_DMS_2014.out
H2CO_DMS_2014.params (http://mnras.oxfordjournals.org/lookup/suppl/doi:10.1093/mnras/stv091/-/DC1).

Please note: Oxford University Press are not responsible for the content or functionality of any supporting materials supplied by the authors. Any queries (other than missing material) should be directed to the corresponding author for the article.

This paper has been typeset from a TEX/LATEX file prepared by the author.